PAPER • **OPEN ACCESS**

An investigation from raw components to composite: 3D printed Voronoi lattice core structured sandwich composite with woven glass fiber-epoxy outer layer

To cite this article: Yılmaz Gür *et al* 2025 *Eng. Res. Express* **7** 015522

Engineering Research Express

PAPER

An investigation from raw components to composite: 3D printed Voronoi lattice core structured sandwich composite with woven glass fiber-epoxy outer layer

Yılmaz Gür[1,2], **Ruhan Benlikaya**[3] and **Sare Çelik**[1]

[1] Department of Mechanical Engineering, Balikesir University, Balikesir, Türkiye
[2] Department of Mechanical Engineering, International University of Sarajevo, Sarajevo, Bosnia and Herzegovina
[3] Department of Secondary Science and Mathematics Education, Balikesir University, Balikesir, Türkiye

E-mail: ygur@ius.edu.ba

Keywords: Voronoi, 3D printing, sandwich composite, FTIR, FFF, glass fiber fabric

OPEN ACCESS

RECEIVED
16 July 2024

REVISED
28 December 2024

ACCEPTED FOR PUBLICATION
7 January 2025

PUBLISHED
17 January 2025

Abstract

A key emerging trend in mechanical engineering design involves adopting strategies that build lightweight lattice geometries, particularly for sandwich structures. These structures are characterized by low mass, a significant surface area to volume ratio, high porosity, and suitable mechanical behavior. This study focuses on the fabrication and investigation of thermoplastic polyurethane (TPU) Voronoi lattice core (V-core) structured sandwich composite with woven glass fiber (WGF)-Epoxy outer layer. The TPU V-Core structure was fabricated using the Fused Filament Fabrication (FFF) three dimensional (3D) printing method. Fourier Transform Infrared Spectroscopy (FTIR), Raman Spectroscopy, and Thermogravimetric Fourier Transform Infrared Spectroscopy (TG-FTIR) analyses were used to examine the interactions between the components within the sandwich composite structure. The experimental results demonstrated that the investigated structure has intricate interactions at the interface between the WGF-Epoxy outer layer and the V-core structure. The thermal stability and thermal degradation pathway of the composite and its components were also examined. In addition, three-point bending (TPB) tests were conducted on the sandwich composite and also on the core structures with plain rectangular prism and Voronoi lattice to assess their mechanical behavior.

1. Introduction

In contemporary times, lightweight sandwich structures have gained widespread application across diverse industries, including aerospace, automotive, and construction. This widespread usage is primarily attributed to their exceptional multifunctional properties, such as high flexural stiffness, thermal insulation, and effective energy absorption capabilities [1, 2]. These structures are composed of two main elements: thin solid face-sheets with high flexural stiffness located at the top and bottom surfaces and a relatively thick, lightweight cellular core structure that separates them. The lightweight cellular core structure facilitates the connection between the face sheets with minimal added weight, enhancing bending and buckling resistance, and providing excellent shear stiffness and energy absorption capabilities [3, 4]. Examining the studies related to lightweight structures depending on the main elements above, it has been seen that polymer foams (polypropylene, thermoplastic polyurethane [5], polytropic acid [6], polyvinyl chloride [5, 7], nomex [8] etc), metals (aluminum, copper, steel, etc), and natural materials (wood [5, 7], bamboo [6], etc) and composites [6] are used as core materials. Fiber reinforced polymers (obtained by combining resins such as epoxy, vinyl ester, etc with various materials such as glass fiber, carbon fiber [7, 8], glass fiber [7], etc), metals (aluminum [5, 6], steel [5, 7], etc), and composites [5] have been used as face sheet materials.

Planar geometries [9, 10] and three-dimensional structures (hexagonal honeycomb, lattice structures, corrugated structures, functionally graded structures, etc) [11, 12] have been used in the production of core

materials to optimize the mechanical properties of sandwich composites and to achieve the required properties for different applications. It was stated that the crashworthiness of cellular structures can be improved by introducing graded materials with suitable designs [12].

Advances in three dimensional (3D) printing have enabled fabrications of cellular cores in the 3D geometries, which are impossible to manufacture by conventional engineering methods [13]. Fused Filament Fabrication (FFF) is one of the most popular 3D additive manufacturing technologies for manufacturing lattice-cored sandwich materials [14]. Studies on lightweight sandwich composites of the core materials produced with FFF technology are increasing day-by-day [15, 16].

One of the lattice structures produced by FFF depends on Voronoi diagrams [17, 18]. The diagrams described by Dirichlet (1850) and Voronoi (1908) are prevalent in various natural models and recognized as among the fundamental topologies established by a given set of points [19]. They are versatile geometric structures and algorithms that find applications in various fields due to their ability to efficiently model spatial relationships and proximity. Voronoi lattice core structures offer a compelling combination of structural efficiency, lightweight design, and versatility, making them valuable in diverse applications across various industries. The Voronoi diagram's simplicity and effectiveness make it a valuable tool for spatial analysis, contributing to advancements in numerous scientific and practical fields. They are used in biology to analyze habitats and distribution patterns [20, 21], applied in the study of crystal structures and materials [22, 23], utilized for weather pattern analysis and spatial modeling [24, 25], and in the robotic industry [26], in the analysis urban spaces [27], in the field of architecture for site analysis and spatial planning [28]. Constructing three-dimensional Voronoi tessellations is a powerful technique for spatial analysis and modeling, and it finds applications in a wide range of scientific and engineering disciplines.

The use of the Voronoi lattice in TPU core structure will offer significant advantages in terms of the mechanical properties, functionality, and sustainability of resulting composites as TPU known for its flexibility and durability is suitable for applications where impact resistance and elasticity are crucial. For these reasons, investigations in this area will contribute to the development of lighter, stronger, and smarter composites in the future. This study investigates the application of digital techniques in the design and fabrication of a creative TPU Voronoi lattice core (V-core) structure produced using additive manufacturing, and its' sandwich composites bonded via epoxy adhesive resin with woven glass fiber (WGF)-Epoxy outer surface layers. The sandwich composite was subjected to Fourier Transform Infrared Spectroscopy (FTIR), Raman Spectroscopy and Thermogravimetric Fourier Transform Infrared Spectroscopy (TG-FTIR) analyses to comprehend the interactions between its components. TG analysis was also used to examine the composite and its components in terms of thermal stability and degradation pathway. In addition, a three-point bending (TPB) test was performed to evaluate the structure's mechanical performance.

2. Experimental

2.1. Materials

Bisphenol-A type vinyl ester (BAVE) Polives 701 resin, supplied by Poliya, Istanbul, Turkey, was used as the bonding material in the study. Vinyl ester resins combine the advantageous properties of both polyester and epoxy resins, offering high mechanical strength comparable to epoxy resins while maintaining the ease of application associated with unsaturated polyester resins. These resins are highly resistant to impact and fatigue, exhibit low water absorption, and possess greater hydrolytic resistance than polyester resins. Additionally, their unique structure ensures high flexural and tensile strength. Polives resins are particularly effective at wetting glass, carbon, and aramid fibers due to their distinct chemical composition. The material properties of Polives 701 resin include a tensile strength of 80 MPa, elongation at break of 5.5%, flexural strength of 160 MPa, Barcol hardness of 35 Barcol, and volumetric shrinkage of 7,7%.

Unidirectional woven glass (UDWG) fiber Metyx EC 330 g m^{-2} was provided by Dost Kimya Industrial Raw Material Industry & Trade Co., Istanbul, Turkey. It was employed as the face sheet material to enhance the flexural and impact strength of the V-core sandwich composite. The fiber is ideal for manufacturing structural laminates with epoxy, polyester, urethane-acrylate, or vinyl ester resins.

Thermoplastic polyurethane (TPU) flexible filament, produced by Polymer Technologies Inc., Yalova, Turkey was used for the 3D printing of the V-core structure. TPU's very soft nature ensures excellent layer-to-layer adhesion and remarkable durability. It is commonly used for applications requiring flexibility or bending during operation. TPU provides an optimal balance of elasticity, rigidity and flexibility making it an ideal material for this purpose.

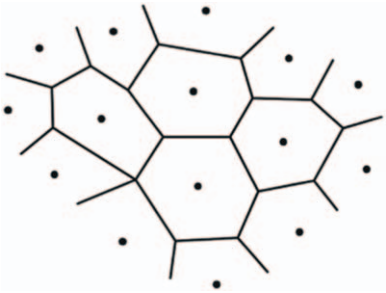

Figure 1. 2D Voronoi diagram.

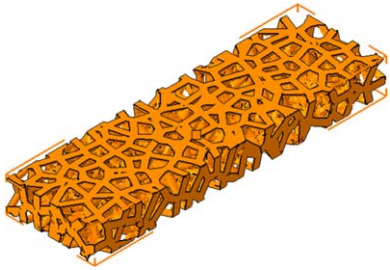

Figure 2. Generated 3D V-core structure.

2.2. Design and fabrication process

The Voronoi diagram is a spatial segmentation algorithm based on Cartesian segmentation, first developed by G. Voronoi [21, 22]. It divides a space into convex polygons (cells) based on proximity to a set of seed points. In a two-dimensional (2D) plane, constructing a Voronoi diagram involves connecting cell points to form triangles and then using perpendicular lines to find circumcenters. Connecting these circumcenters creates the boundaries of the Voronoi cells. The process applies to establishing convex fields around seed points, forming polygons that encompass areas closer to a particular seed point than any other. Voronoi cells are convex polygons generated by connecting points equidistant between two seed points, establishing boundaries that divides the space into regions associated with each seed point. The concept of circumcenters and perpendicular lines is essential for defining the boundaries of Voronoi cells, ensuring that the cell boundaries are equidistant from the seed points (see figure 1).

Constructing 3D Voronoi tessellations involves distributing seed points in 3D space and generating cells around these points, forming 3D shapes with flat sides. This process extends the concept of the 2D Voronoi tessellation into three dimensions.

The design and fabrication process of the 3D printed Voronoi lattice core structure consisted of several key steps. First, a 3D model of the desired lattice structure was created using computer-aided design (CAD) software. The design space was then divided into individual unit cells, and seed points and beam radius values were calculated for each unit cell [29]. These seed points and beam radius values were subsequently used to generate the Voronoi tessellation, forming the lattice structure (see figure 2). For this structure, the beam thickness was set to 4 mm, the number of random seeds points was 50, and the point spacing was 10 mm. The design was developed using nTop computational design software. The volume of the Voronoi core structure and the volume fraction ratio were calculated as 82475mm^3 and %34 respectively.

This lattice structure was then fabricated with a 3D printer using (FFF) technology, which allows for the precise and controlled deposition of material layer by layer, to create complex geometries [30].

2.2.1. 3D printing of the V-core structure

The fabrication process began with the 3D printing of a Voronoi-structured rectangular prism measuring 60 × 20 × 200 mm. FFF was employed to manufacture this structure. 3D printing parameters for the fabrication of TPU V-core structure are detailed in table 1. A hardened steel nozzle was used to maintain the diameter of the nozzle's orifice as 0.4 mm. The V-core structure was fabricated using a Flash Forge Creator 3D FFF printer, with the TPU filament of 1.75 mm in diameter.

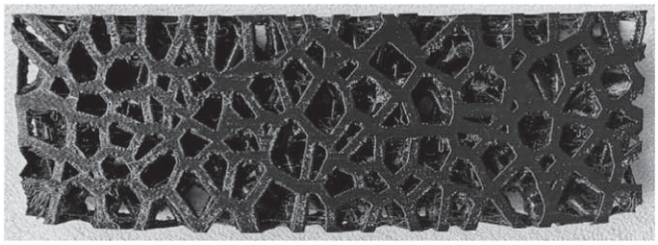

Figure 3. 3D printed TPU V-core structure.

Table 1. 3D printing parameters of TPU V-core.

Nozzle temperature	250 °C
Number of outer walls	3
Nozzle diameter	0.4
Nozzle material	Hardened steel
Printing speed	30 mm s^{-1}
Bed temperature	60 °C
Layer height	150 μm
Filament material	TPU
Infill ratio	%15
Retraction rate	4mm
Top Bottom layer count	4
Infill pattern	Linear
Filament diameter	1.75

The layer thickness was set to 150 μm. during the fabrication of the V-core structure, with the build platform temperature was maintained at 100 °C. The 3D printed TPU V-core structure is shown in figure 3. The incorporation of V-core structures in the fabrication of sandwich composites represents a significant advancement in material engineering and manufacturing processes [31].

2.2.2. WGF-Epoxy covered V-core sandwich composite panel

The composite panel comprised two layers of WGF enclosing the additively manufactured TPU of V-core structure. Bonding of both components was achieved using an epoxy adhesive. Epoxy resin was applied to the upper and lower surfaces of the TPU V-core structure to ensure a robust bond with the WGF fabric layer. Subsequently, the WGF layer was placed onto the TPU V-core structure, and rolling pressure was applied to facilitate the penetration of epoxy resin into the glass fiber layer. The adhesive application plays a critical role in forming a durable connection between the polymer core structure and the cover layer made of WGF fabric. This sequence (figure 4) repeated twice for both the upper and lower surfaces to fortify the strength of the TPU V-core to ensure a strong bond between the layers.

The resulting sandwich composite was shown in figure 5. The combination of these materials adds strength and durability to the lattice structure while preserving its lightweight properties. The 3D printed V-core structure with woven glass fabric top and bottom faced sandwich composite exhibits high specific strength and stiffness, making it an excellent choice for applications requiring reduced weight and strong structural integrity.

The primary objective of this design is to optimize the load distribution across the entire cross-section. Bending moments result in normal stresses within the cover layers, whereas transverse forces induce shear stresses in both the core and adhesive joint.

2.3. Characterization of the sandwich composite

FTIR analysis of the sandwich composite was conducted using a Perkin Elmer Spectrum Two (PerkinElmer Inc., Massachusetts, USA) spectrometer. The analysis was performed in the range of 400–4000 cm^{-1} with Attenuated Total Reflectance (ATR) technique to characterize the chemical composition of the components (the TPU filament, the epoxy matrix and the WGF) and the interactions within the composite. A 2mm thick cross section of the sandwich composite sample was placed on the ATR crystal to analyze regions identified as (I) TPU V-core, (II) WGF-Epoxy, and (III) the interface between I and II, ensuring good contact between the sample and the crystal (see figure 6).

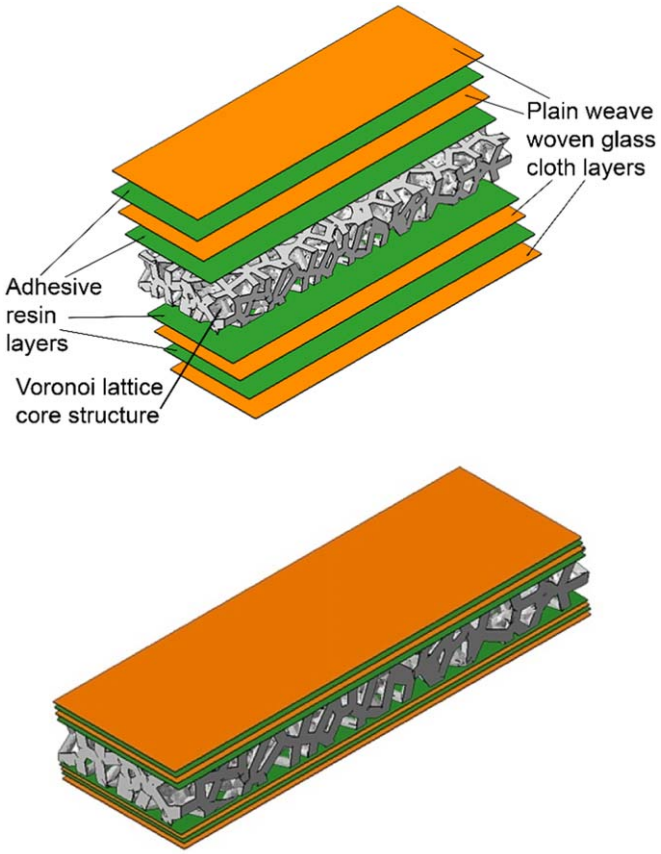

Figure 4. Representation of V-core structured, WGF-Epoxy layer top and bottom faced sandwich.

Figure 5. V-core structured WGF-Epoxy layer top and bottom faced sandwich.

Thermal stabilities and degradation pathways of the samples were also analyzed using a Perkin Elmer Pyris STA 600 thermogravimetric analyzer (PerkinElmer Inc., Massachusetts, USA) and Spectrum 1 FTIR Spectrometer. The analyses were performed under a nitrogen atmosphere with heating rate of 10 °C min^{-1} over a temperature range of 50–600°C. These tests provided insight into the interactions between the composite's components.

To further investigate the interface in region III, Raman depth profiling was conducted using a Renishaw in VIA Dispersive Raman Spectrometer. A diode laser with wavelength of 785 nm (300 mW power) was focused on the sample through a 20× microscope objective lens. Raman scattering was recorded with a grating of 1200 grooves/mm, using an exposure time of 10 seconds per spectrum to produce high-resolution Raman images.

Three-point bending (TPB) tests were performed on the V-core structure, a plain rectangular prism core and the V-core structured composite sandwich in accordance with the EN ISO 178 standard. Testing was carried out at room temperature (~20 °C) using a Zwick/Roell universal testing machine (Zwick/Roell GmbH, Ulm, Germany) [32]. A makroXtens BT2-EXMACRO.H11 type extensometer produced by Zwick/Roell GmbH, Ulm, Germany was used to measure the displacement of the specimen under the bending load. A constant loading speed of 1 mm min^{-1} was applied during the bending test, and the reaction force and a displacement of the compression platens were recorded.

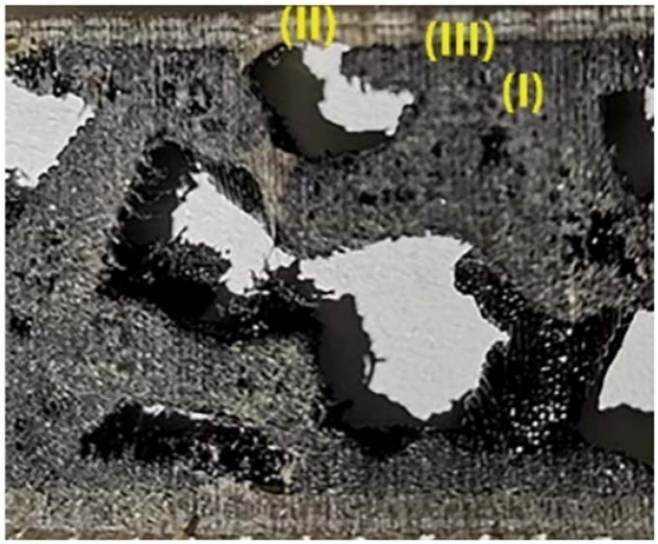

Figure 6. 2 mm thick cross-section of TPU V-core composite.

3. Results

3.1. FTIR analysis

Figure 7 represents the FTIR spectra of the raw components in the sandwich composite: WGF fabric, the TPU filament and the epoxy matrix. The FTIR spectrum of the WGF fabric (1) in figure 7 shows a peak between 3200–3600 cm^{-1}, which corresponds to O–H stretching bonded to C or Si. Peaks between 2800–3100 cm^{-1} are attributed to C–H stretching in CH, CH_2 and CH_3 (aromatic or aliphatic groups), while the 1050–1100 cm^{-1} range corresponds to Si–O–Si stretching [33]. A peak at 1243 cm^{-1} is attributed to C–O asymmetric stretching or C–O–C stretching on the fabric surface. Additionally, the peak at 1712 cm^{-1} is associated with the carbonyl group, likely originating from surfactants or antistatic agents added to the WGF [34]. The observed peaks indicate that the WGF fabric contains not only Si-O groups but also functional groups with organic content. Deng et al [35] stated that glass fiber surfaces modified by alkali treatment, acetylation, electroplating, plasma treatment, and grafting are commonly used to improve the interfacial adhesion between glass fibers and epoxy. In the FTIR spectrum of the TPU filament (2), peaks around 3330 cm^{-1} (hydrogen bonded –N–H stretching), between 2800–3100 cm^{-1} (C-H), at 1528 cm^{-1} (–N–H deformation), and 1727 cm^{-1} (–C=O) confirm the presence of a urethane group. The peak at around 1700 cm^{-1} corresponds to carbonyl stretching of the hydrogen-bonded urethane group. Polyurethanes can form hydrogen bonds due to the N–H donor group and the C=O acceptor group in the urethane bond [36]. A peak at 1596 cm^{-1} is attributed to N–H bending and C=C stretching [37]. The FTIR spectrum of the epoxy matrix (3) shows the presence of an O–H group with a broad band at 3369 cm^{-1}, C–H stretching between 2800 and 3000 cm^{-1}, C=C (1608 cm^{-1}) and C–C (1508 cm^{-1}) stretching in aromatics, C–O or C–O–C stretching at 1243 cm^{-1}, and C–O–C stretching in ethers at 1034 cm^{-1} [34, 38].

Figure 8 shows the FTIR spectra of the V-core structure (I), WGF-epoxy laminated outer layer (II), and the interface (III) between them. When comparing the FTIR spectra of the V-core structure (I) in figure 8 with that of the TPU filament (2) in figure 7, a shift from 3329 to 3325 cm^{-1} in the band attributed to the N–H stretching and some changes between 2800–3000 cm^{-1} are observed. These shifts suggest probable interactions between the polymer chains during the melt extrusion printing process of the TPU filament into the V-core structure. The most significant shifts are observed in the N-H and C-H stretching regions. FTIR spectrum of the WGF-Epoxy layer (2) in figure 8 contains peaks from both WGF and the epoxy matrix in the range of 1280–1800 cm^{-1}. However, significant shifts are seen between 1000 and 1280 cm^{-1}, along with new band/peaks at 3255, 2928, 1107, and 943 cm^{-1}. The carbonyl peak at 1712 cm^{-1} in the WGF structure, in figure 7, shifts to a higher wavenumber (1718 cm^{-1}) in the WGF-Epoxy layer. These changes indicate the formation of bonds or interactions involving the Si–O, –OH, –CH, and C–O groups between the epoxy matrix and the WGF fabric, as shown in figure 9.

Some significant changes in the range of 1000–1300 cm^{-1} are observed in FTIR spectra of the interface (III) of the sandwich composite. The new peak at 1261 cm^{-1} is seen at the interface while there are the peaks at 1220 cm^{-1} in the FTIR spectrum of the V-core, at 1234 cm^{-1} in that of the WGF-Epoxy layer in figure 8(a), and

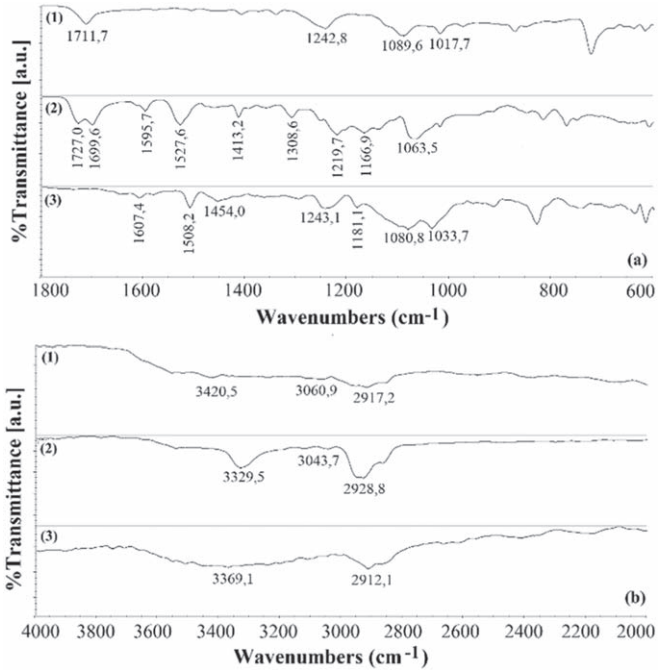

Figure 7. FTIR spectra of raw components in the sandwich composite: The WGF fabric (1), the TPU filament (2), the epoxy matrix (3) samples in the ranges of 600–1800 cm^{-1} (a) and 2000–4000 cm^{-1} (b).

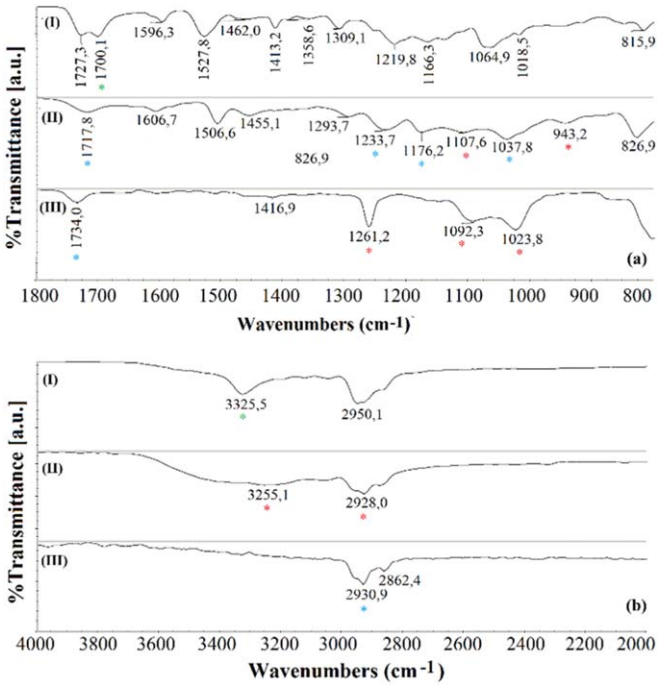

Figure 8. FTIR spectra of the V-core structure (I), the WGF-Epoxy layer (II) at the composite, and the interface (III) between them in the ranges of 800–1800 cm^{-1} (a) and 2000–4000 cm^{-1} (b) **Significant changes (new peaks in red, shifted peaks in blue, the peaks disappearing at the interface or the layer in green) are marked.*

at 1243 cm^{-1} that of Epoxy in figure 7(a). There have been similar observations also for the peaks at 1093 and 1023 cm^{-1} at the interface. The regions in the range of 3600–3100 cm^{-1} and of 1600–1400 cm^{-1} in the FTIR spectra of both components (I, II) appear smoother at the interface. Additionally, two carbonyl peaks at 1727 and 1700 cm^{-1} in the V-core structure merge into a single peak at 1734 cm^{-1} at the interface. It means that the concentration of non-hydrogen bonded (free) N–H [39] and C=O groups in the V-core structure increases after interacting with epoxy. It is conceivable that the hydrogen bonding (figure 10(a)) between the rigid

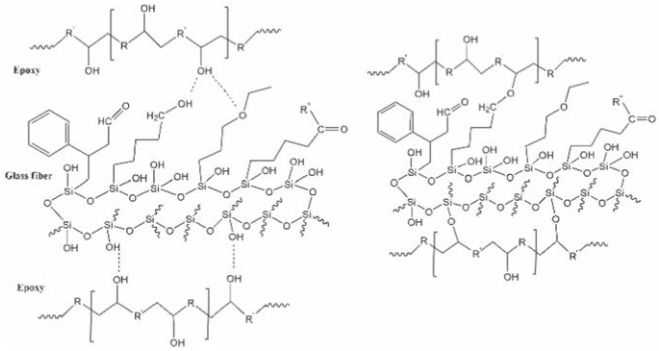

Figure 9. Possible interactions and bonding between the epoxy matrix and the WGF fabric.

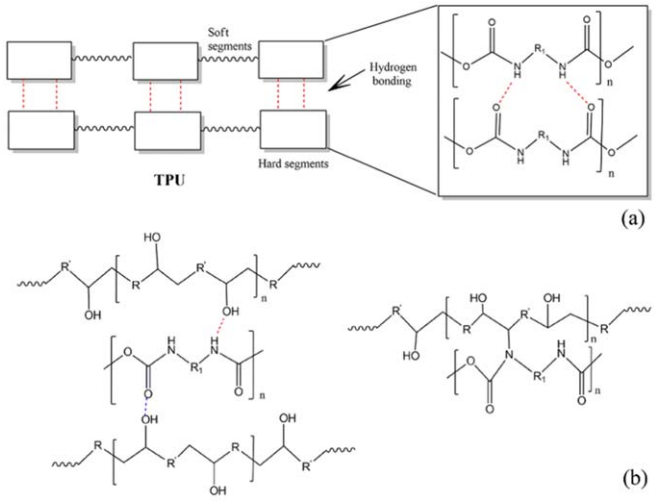

Figure 10. (a) Interactions in the hard segment involving urethane group at the structure of TPU, (b) Possible interactions and bonding between the epoxy and the V-core.

segments in the structure of the V-core weakens after interaction with the epoxy, as was observed in a similar study where PEO was mixed with TPU. It was stated that the –NH group in TPU chains and the –C–O–C- group in the PEO chain could form the hydrogen bond interaction [40]. All changes mentioned above can imply the formation of the new interactions and/or bonds involving the C–O/C–N, C=O, N–H, and –OH groups at the interface between the epoxy layer and the V-core structure. Possible interactions/bonding at the interface are shown in figure 10(b), depending on figures 7 and 8. In addition to figure 10(b), the carbonyl group at the interface may repel the C–O–C group in the structure of R/R' of the epoxy.

3.2. Raman analysis

Figure 11 shows the Raman spectra of the WGF-epoxy layer and the interface between the layer and the V-core structure. The peaks at 639, 1114 and 1186 cm^{-1} (C–C stretching) and at 1603 cm^{-1} (stretching of phenyl ring) [41], at 3059 cm^{-1} (=C–H stretching of the aromatic ring) can belong to the epoxy matrix in the spectrum of the layer. Peaks at 1001 cm^{-1} (Si–O) and 1695 (C=O) confirm the presence of WGF in the layer. In the Raman spectrum of the interface, peaks at 638 and 1184 cm^{-1} are consistent with those of the epoxy. The band at 1726 cm^{-1} corresponds to 'free' carbonyl groups. The band at 1700 cm^{-1}, corresponding to the ordered hydrogen-bonded species in the hard segment, is not observed in the regarding spectrum. This band is also absent in the FTIR spectrum of the interface in figure 8(a). The band at 2912 cm^{-1} is observed in the Raman spectrum of the interface instead of the bands at 2922 and 2871 cm^{-1} observed in that of TPU in other studies [42, 43]. The peak at 867 cm^{-1} represents C–C and C–O stretching [42]. While Raman peaks observed at 1313, 1617, and 1436 cm^{-1} for TPU in this study, they are observed at 1308, 1614, and 1442 cm^{-1} at the interface in other studies. However, a peak at 1387 cm^{-1}, present in the interface spectrum, is not observed in the spectra of either the WGF-epoxy layer or TPU in prior studies. It was stated in another study that the N–H stretching modes are typically observed in the 3130–3445 cm^{-1} region of infrared and Raman spectra. However, in Raman

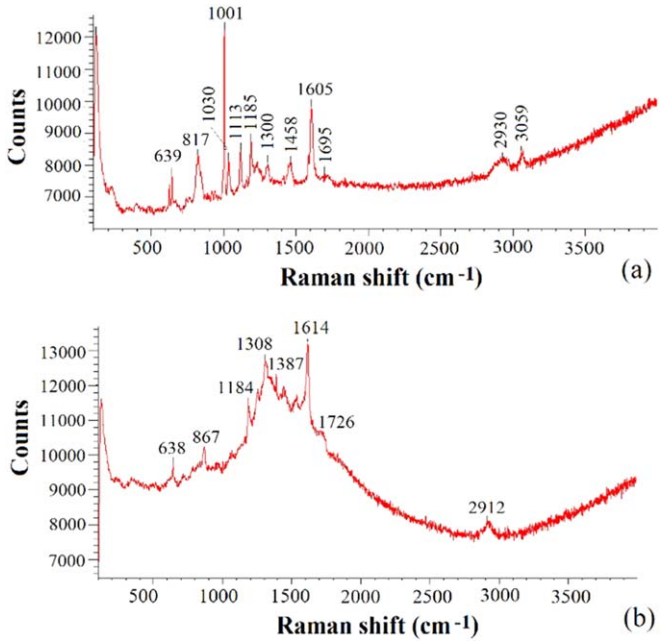

Figure 11. Raman spectra of the WGF-epoxy layer and the interface region.

spectra, the non-hydrogen bonded N–H stretching mode is either rarely present or extremely weak due to insufficient polarizability [44]. The mode is also absent in the Raman spectrum of the interface. Based on the data obtained from the Raman spectra, it can be concluded that interactions or bonds have formed between the components of the sandwich composite.

3.3. Thermogravimetric analysis

Thermogravimetric (TG) and Derivative Thermogravimetric (DTG) curves of the sandwich composite and of its' components are shown in figure 12. In addition, the data related to these thermal analyses is summarized in table 2. With the addition of WGF to the epoxy, an increase in the residue value (%) and a slight improvement in thermal stability are observed as seen in figure 12 and table 2.

The residue value (%) and thermal stability of the sandwich composite lie between those of the V-core and the epoxy. Figure 13 illustrates the TG-FTIR spectra captured at three key stages of thermal degradation based on the DTG curves for the epoxy and the WGF-Epoxy layer: the onset of degradation (2005 s), the maximum degradation rate Tmax, (~2400 s), and the end of degradation (~2700 s). Both similarities and differences are observed in these spectra. The differences suggest that these materials exhibit distinct types and quantities of degradation products, as well as differing thermal degradation pathways. A previous study [45] noted that the presence of synthetic fiber reinforcements influences the thermal decomposition process, pyrolysis kinetics, and combustion behavior of epoxy resins. In addition, another study investigated the pyrolysis characteristics of epoxy glass fiber reinforced plastics at varying heating rates (5, 10, 15, and 20 °C min^{-1}) from 25 to 1000 °C identified the main volatile products as H_2O (3736 cm^{-1}), CO_2 (2360, 2344, 2310 and 670 cm^{-1}), carbonyl components (1794 cm^{-1}), and aromatic components (1510 cm^{-1}) during the thermal degradation [46]. These peaks corresponding to the main volatiles are also present in figure 13. It can be inferred that the WGF retards the release of these volatiles during the thermal degradation of the epoxy. This behavior is likely attributed to the possible interactions or bonds depicted in figure 9.

TG-FTIR spectra captured at key time intervals encompassing the onset of thermal degradation (1544 and 1633 s), the first T_{max} (~1900 s), the second T_{max} (~2200 s), and the end of thermal degradation (2830 and 2646 s) from the DTG curves of the sandwich composite and of the V-core structure are presented in figure 14.

Petrović *et al* (1994) reported that the initial weight loss during thermal degradation of segmented polyurethanes is associated with the degradation of the hard segment, while the second weight loss is attributed to the decomposition of the soft segment [47]. In the study by Cervantes-Uc *et al* [48], peaks at 2926 and 2859 cm^{-1}, as well as at 2357 and 2310 cm^{-1} during the first stage of degradation, were linked to hydrocarbon fragments (C–H stretching vibrations) and CO_2 formation, respectively. The formation of CO_2 ascribed to the breakdown of urethane groups. A small band at 1092 cm^{-1} was associated with C–O stretching vibrations, and broad band in the 4000–3500 cm^{-1} range was associated with O–H stretching vibrations from water or hydroxyl-terminated compounds, as well as N–H stretching vibrations from urea or amine groups. During the

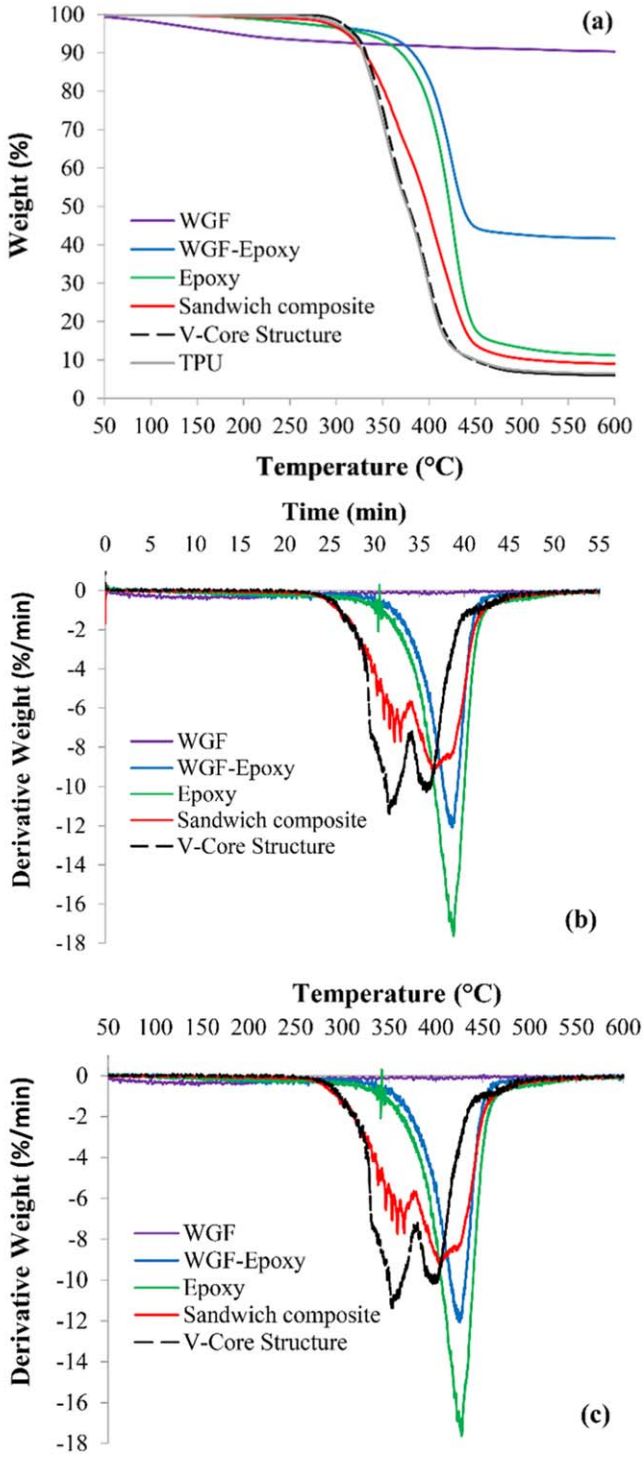

Figure 12. (a) TG and (b, c) DTG curves of the sandwich composite and its' components.

Table 2. The data obtained from TG and DTG curves of the sandwich composite and its' components.

Samples	Residue (%)	T_{10}	T_{20}	T_{50}	T_{80}	T_{max} (DTG) [°C]
WGF	90,3	>600	—	—	—	150
Epoxy	11,2	369	395	422	446	428
WGF-Epoxy	41,6	382	405	436	—	426
V-core structure	6,4	332	345	378	412	353,397
TPU filament	5,9	328	342	376	410	352,396
Sandwich composite	8,9	330	352	398	435	360,404

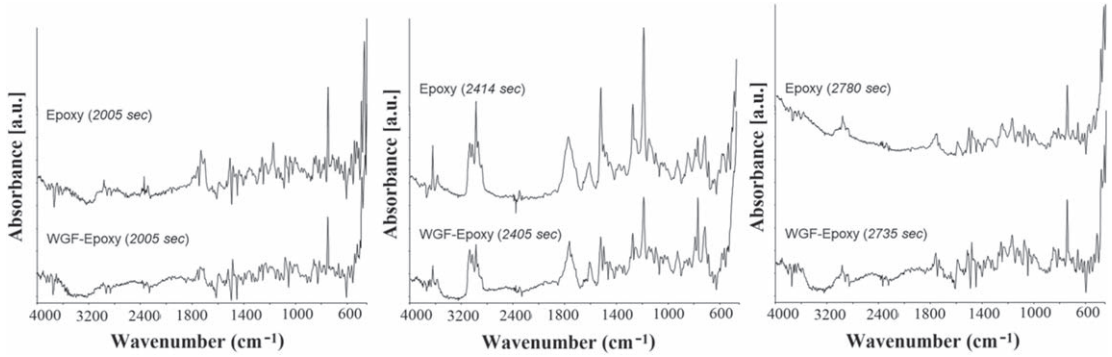

Figure 13. TG-FTIR spectra of the epoxy and the WGF-Epoxy layer at various times during their degradation.

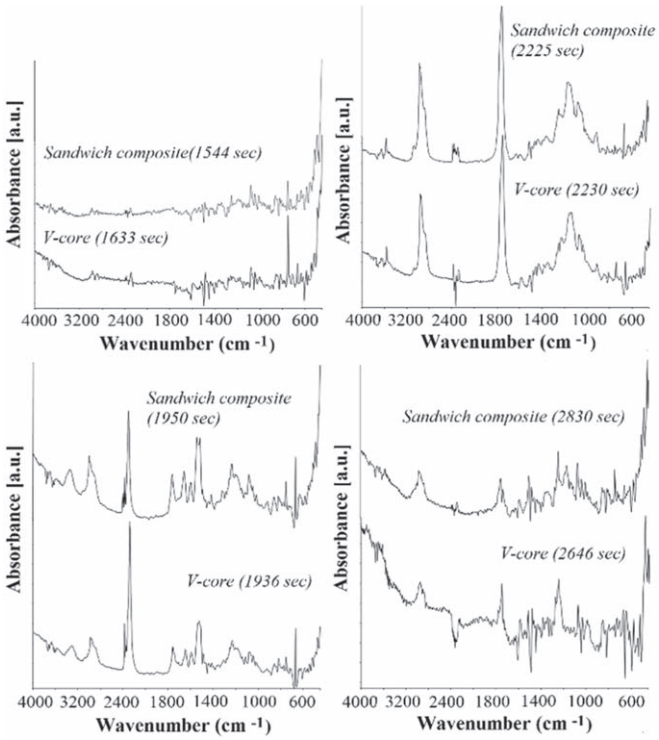

Figure 14. TG-FTIR spectra of the V-core structure and the sandwich composite at various times during their degradations.

second stage, bands at 2942 and 2867 cm^{-1} and at 1450 and 1370 cm^{-1} were observed, corresponding to C–H stretching vibrations in methylene and methyl groups. Additionally, a carbonyl band at 1743 cm^{-1}, and a band at 1112 cm^{-1} linked to C–O vibration of the ether group were observed [48]. The findings of this study align with those of Cervantes-Uc *et al* [48] in several respects. Peaks corresponding to hydrocarbon fragments and CO_2 formation are observed during the first degradation stage of both the V-core structure and the sandwich composite. Notably, the peak observed between 3200 and 3600 cm^{-1} is attributed to the formation of amine groups, which result from the removal of CO_2 from the urethane group.

The formation of structures containing aromatic, carbonyl, amine and ether groups is evident in the peaks observed between 1000 and 1800 cm^{-1}. While the removal of CO_2 from the sandwich composite occurs slower more slowly compared to the V-core, the formation of amine and carbonyl group structures progress more rapidly in the composite. The second stage degradation products of the V-core and the sandwich structure are almost identical, as this phase corresponds to the degradation of the soft segment in TPU. The presence of different products is clearly visible at the end of their thermal degradations. All the above mentioned observations can support the presence of the interactions or bonding between the hard segment in the V-core and the epoxy in the sandwich composite, as illustrated in figure 10(b).

Figure 15. Three-point bending test of the composite.

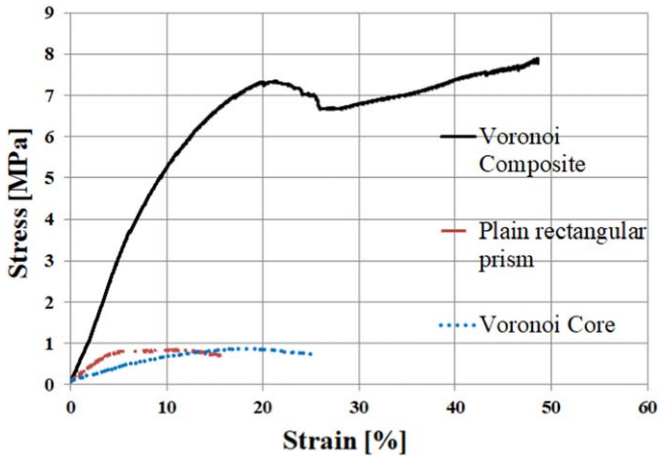

Figure 16. Three-point bending test of the V-core structured composite, and plain and Voronoi core structures.

3.4. Mechanical analysis

3.4.1. Three-point-bending test of the composite

The TPB test rig for TPU V-core structured composite sandwich test specimen can be seen in figure 15.

The stress–strain diagram of the 3P bending test for the Voronoi composite structure is depicted in figure 16. Initially, the stress increases linearly with strain in the early part of the curve (0%–5% strain), indicating elastic deformation. During this phase, the material returns to its original shape upon the removal of the load. The stress reaches its maximum value of approximately 7,3 MPa at around 20% strain, marking the ultimate tensile strength (UTS). This represent the maximum stress the material can withstand before undergoing significant permanent deformation. Following the peak, the stress experiences a noticeable drop, signifying the formation of micro-cracks typical of composite structures. Following the drop, the curve shows a relatively steady region (25%–40% strain), where the stress slightly fluctuates and gradually increases. This phase likely corresponds to strain hardening and stabilization as the material undergoes plastic deformation. Beyond 40% strain, the stress gradually rises again, suggestion a combination of hardening mechanisms and resistance to further damage leading up to eventual failure. The elastic stiffness, peak strength, and post-peak behavior are influenced by the Voronoi pattern's geometry and the material properties of the composite structure. The observed stabilization and gradual hardening post-peak reflect the ability of the composite to redistribute stresses effectively, a key characteristic of energy-absorbing cellular structures.

When the TPU made Voronoi composite structure is compared to TPU made plain rectangular prism and Voronoi core structures, it exhibits superior mechanical properties in terms of stiffness, ultimate strength, and ductility, making it the most robust and energy-absorbing system.

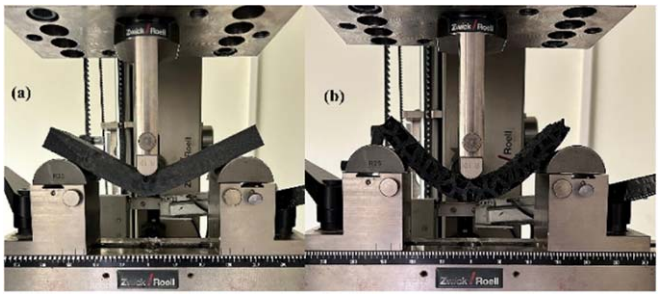

Figure 17. Three-point bending test of TPU core structures (a) plain rectangular prism (b) Voronoi lattice core.

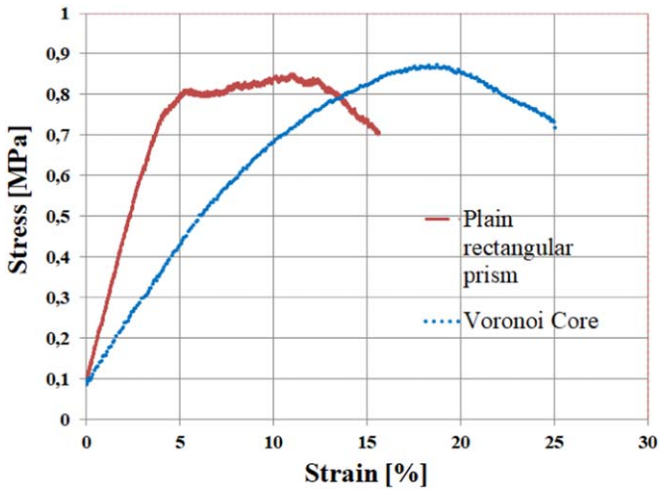

Figure 18. Three-point bending test diagram of TPU based plain rectangular prism and Voronoi core structures.

3.4.2. Three-point bending tests of TPU based rectangular prism and V-core structures

To reveal the contribution of the Voronoi core structure to improve the mechanical properties of the composite, the bending properties of this core structure were compared with those of the core structure in the form of a rectangular prism printed with the same volume as the V-core. Therefore, a three-point bending test was also carried out to the TPU made plain rectangular prism (figure 17a) and Voronoi lattice core (figure 17(b)) structures.

The stress–strain diagram of the bending specimens is given in figure 18. This stress–strain diagram provides a comparative analysis of the mechanical responses of two TPU-based structures: a Voronoi core structure depicted as a dotted line and a plain rectangular prism depicted as a line in this figure.

The stress–strain curve for the plain rectangular prism, represented by a solid line, begins with a sharp increase in stress, reaching a peak of approximately 0.81 MPa at around 5% strain. Following this peak, the stress levels off and shows some fluctuations but generally maintains a high-stress level with minor decreases up until around 11% strain. This plateau indicates that the TPU made rectangular prism can sustain a relatively stable load after initial yielding, which suggests a certain level of ductility or plastic deformation capacity. After 11% strain, the stress starts to decline gradually, indicating progressive material failure.

The stress–strain curve for the Voronoi structure, represented by a dotted line, exhibits a more gradual increase in stress compared to the rectangular prism, reaching its peak at around 0.87 MPa at approximately 18% strain. This indicates that the Voronoi structure has a higher initial stiffness, likely due to its complex, irregular geometry which can distribute stress differently across the structure. After reaching peak stress, the Voronoi structure's stress gradually decreases, indicating progressive failure similar to the rectangular prism. However, the failure mode appears more gradual, which may be a result of the load redistributing across different sections of the Voronoi pattern as it deforms.

When both structures are compared, the rectangular prism achieves a slightly lower peak stress (~0.81 MPa) than the Voronoi structure (~0.87 MPa). This suggests that, in terms of absolute strength, the Voronoi structure has a slight advantage over the plain rectangular prism. The Voronoi structure exhibits a more extended range of deformation, reaching a peak strain of approximately 18%, while the rectangular prism peaks at around 11% strain.

4. Conclusion

The 3D printed V-core structured sandwich composite, made with woven glass fabric top and bottom-faced layers, demonstrates high specific strength and stiffness. It is well-suited for applications requiring weight reduction and structural integrity. The utilization of V-core structures in composite sandwich fabrication represents a significant advancement in material engineering and manufacturing processes. This type of sandwich panel can be utilized in the aerospace industry with various core materials, as the face sheets of the V-core structure are composed of WGF fabric reinforcement and coated with epoxy resin.

Globally tessellating all seed points and cylindrical edging with corresponding beam radius values in the design space allows for the creation of intricate 3D V-core structures that possess optimized mechanical properties and unique geometries. Understanding the future trends in 3D printing of V-core structures will provide valuable insights into the evolving landscape of additive manufacturing and its impact on sandwich composites.

The findings suggest the intricate interactions occurring at the interface between the WGF-Epoxy laminated outer layer and the TPU V-core structure. The FTIR, Raman, and TG-FTIR analyses provide valuable insights into the chemical composition and/or potential interaction/bonding mechanisms within the sandwich composite. Furthermore, the shifts in peaks and the emergence of new peaks at the interface hint at the formation of novel interactions and bonds. This detailed examination not only sheds light on the composition of the interface but also provides a deeper understanding of the bonds or interactions formed within the hybrid lattice sandwich structures.

It was seen from TG curves that the sandwich composite has the best thermal stability between the epoxy, WGF-Epoxy and the V-core structure. The interaction of the hard segment in the V-core structure with the WGF-epoxy layer at the interface of the composite caused some changes, especially in the first step degradation of TPU.

The stress–strain behavior of the composite sandwich structure under three-point bending was analyzed. Initially, a peak stress of 7,3 MPa was observed at approximately 20% strain, indicating the onset of linear elastic behavior. The stress–strain behavior of the TPU made V-core structured composite highlighted the strengths and limitations of the composites. The initial high strength is advantageous, but the structure undergoes progressive localized failures after reaching peak stress. The residual strength after major failure indicates a degree of toughness, which may be useful in applications where some structural integrity is needed even after initial damage. Adjusting the Voronoi pattern or material properties might improve the post-peak behavior and reduce the sharp declines.

Furthermore, another three-point bending test is also carried out in order to compare the bending behaviors of the plain rectangular prism and the Voronoi core structures. The results indicate that the Voronoi structure can endure more strain before reaching its peak, reflecting better energy absorption and greater toughness. The rectangular prism demonstrate the ability maintains a relatively stable load after its initial yielding, while the Voronoi structure has a gradual load drop after peak stress. This difference suggests that the Voronoi structure may offer better energy dissipation, potentially making it more resilient to impacts or repeated loads, where gradual failure is preferred over sudden failure.

Declaration of competing interest

The authors declare that there is no conflict of interest.

Acknowledgments

There is no funding from outside. The authors thank METU Central Laboratory for TG-FTIR and Raman analyses.

Data availability statement

The data cannot be made publicly available upon publication because no suitable repository exists for hosting data in this field of study. The data that support the findings of this study are available upon reasonable request from the authors.

ORCID iDs

Yılmaz Gür https://orcid.org/0000-0003-1709-1298
Ruhan Benlikaya https://orcid.org/0000-0002-1731-8846
Sare Çelik https://orcid.org/0000-0001-8240-5447

References

[1] Schaedler T A and Carter W B 2016 Architected cellular materials *Annu. Rev. Mater. Res.* **46** 187–210
[2] Carlsson L A and Kardomateas G A 2011 Structural and failure mechanics of sandwich composites *Springer Science & Business Media* **121** 19–37
[3] Gibson L J and Ashby M F 1999 *Cellular solids: Structure and properties* (Cambridge University Press)
[4] Allen H G 2013 *Analysis and Design of Structural Sandwich Panels: The Commonwealth and International Library: Structures and Solid Body Mechanics Division* (Elsevier)
[5] Palomba G, Epasto G and Crupi V 2022 Lightweight sandwich structures for marine applications: A review *Mechanics of Advanced Mater. Struc.* **29** 4839–64
[6] Njim E, Raad H, Jweeg M, Al-Waily M, Hameed A, Youssef A and Elsayed F 2024 Mechanical properties of sandwiched construction with composite and hybrid core structure *Adv. Polym. Tech.* **2024** 1–14
[7] Ma Y, Cui X, Huang M, Zhang N, Gao G and Liu S 2023 High erosion resistance thermoplastic polyurethanes composites fabricated via intercalation reinforced interfacial interaction *J. Appl. Polym. Sci.* **141** e55021
[8] Ramnath V, Alagarraja K and Elanchezhian C 2019 Review on sandwich composite and their applications *Mater. Today Proc.* **16** 859–64
[9] Sugiyama K, Matsuzaki R, Ueda M, Todoroki A and Hirano Y 2018 3D printing of composite sandwich structures using continuous carbon fiber and fiber tension *Composites* A **113** 114–21
[10] Kim B-J, Kim J, Cha S-H, Shim Y-B, Jeong C, Kim N and Park Y-B 2021 Interfacial enhancements between a three-dimensionally printed honeycomb-truss core and woven carbon fiber/polyamide-6 face sheets in sandwich-structured composites *Composites* A **149** 106534
[11] Yu R, Liu J, Luo W and He W 2018 Effects of geometric configurations of corrugated cores on the local impact and planar compression of sandwich panels *Composites* B **152** 324–35
[12] Lu C, Cao Y, Wu W, Li S, Wang Z and Hou S 2023 A novel design method of circular sandwich panels with gradient continuous controllable core based on space-filling design and 2D-Voronoi method *Mater. Today Commun.* **36** 106750
[13] Bitzer T 2012 *Honeycomb Technology: Materials, Design, Manufacturing, Applications, and Testing* (Springer Science & Business Media)
[14] Sivakumar N, Kaaviya J, Palaniyappan S, Nandhakumar G, Prakash C, dr B and Pandiaraj S 2024 A machine learning approach for predicting flexural strength of 3D printed hexagon lattice-cored sandwich structures *Mater. Today Commun.* **41** 110230
[15] Hashemi M, Hatami O and Tajbakhsh M R 2024 Investigation of the performance of the structure and energy absorption in sandwich panels of PLA/TPU manufactured by the FFF technique *Proc. Inst. Mech. Eng. Part L J. Mater. Des. Appl.* **238** 416–29
[16] Pinho A C and Piedade A P 2021 Sandwich multi-material 3D-printed polymers: influence of aging on the impact and flexure resistances *Polymers* **13** 4030
[17] Alemayehu D B and Todoh M 2024 Enhanced energy absorption with bioinspired composite triply periodic minimal surface gyroid lattices fabricated via fused filament fabrication (FFF) *J. of Manufacturing and Materials Processing* **8** 86
[18] Ahmed A M R M, Mahdi E, Oosterhuis K, Dean A and Cabibihan J-J 2023 Mechanical and energy absorption properties of 3D-printed honeycomb structures with Voronoi tessellations *Front. Mech. Eng.* **9** 1204893
[19] Wadley H N G, Fleck N A and Evans A G 2003 Fabrication and structural performance of periodic cellular metal sandwich structures *Compos. Sci. Technol.* **63** 2331–43
[20] Xiong J, Ma L, Pan S, Wu L, Papadopoulos J and Vaziri A 2012 Shear and bending performance of carbon fiber composite sandwich panels with pyramidal truss cores *Acta Mater.* **60** 1455–66
[21] Aurenhammer F 1991 Voronoi Diagrams—A Survey of a fundamental geometric data structure *ACM Comput. Surv.* **23** 345–405
[22] Voronoi G 1908 Nouvelles applications des paramètres continus à la théorie des formes quadratiques. Deuxième mémoire. Recherches sur les parallélloèdres primitifs *J. für die Reine und Angewandte Mathematik* **134** 198–287
[23] Frayssinet E, Colabella L and Cisilino A P 2022 Design and assessment of the biomimetic capabilities of a Voronoi- based cancellous microstructure *J. Mech. Behav. Biomed. Mater.* **130** 105186
[24] Hoffmann J, Donoughe S, Li K, Salcedo M K and Rycroft C H 2018 A simple developmental model recapitulates complex insect wing venation patterns *Proceedings of the National Academy of Sciences USA* **115** 9905–10
[25] Blatov V A 2004 Voronoi-Dirichlet polyhedra in crystal chemistry: theory and applications *Crystallogr. Rev.* **10** 249–318
[26] Ward L, Liu R, Krishna A, Hegde V I, Agrawal A, Choudhary A and Wolverton C 2017 Including crystal structure attributes in machine learning models of formation energies via Voronoi tessellations *Phys. Rev.* B **96** 024104
[27] Mosca M M and Kurlin V 2020 Voronoi-based similarity 48 distances between arbitrary crystal lattices *Cryst. Res. Technol.* **55** 1900197
[28] Cheung C, Tam C, Leung W N, Ng K and Sze W 2022 Applications of flexible spatial and temporal discretization techniques to a numerical weather prediction model *Proc. of the Platform for Advanced Scientific Computing Conf.* 1–8
[29] Lei H Y, Li J R, Xu Z J and Wang Q H 2020 Parametric design of Voronoi-based lattice porous structures *Mater. Des.* **191** 108607
[30] Liu T, Guessasma S, Zhu J and Zhang W 2019 Designing cellular structures for additive manufacturing using Voronoi–Monte Carlo approach *Polymers* **11** 1158
[31] Kladovasilakis N, Charalampous P, Tsongas K, Kostavelis I, Tzetzis D and Tzovaras D 2021 Experimental and computational investigation of lattice sandwich structures constructed by additive manufacturing technologies *J. Manuf. Mater. Process.* **5** 95
[32] EN ISO 178 2019 Plastics-Determination of flexural properties https://iso.org/standard/70513.html
[33] Schauperl Z, Ivanković L, Bauer L, Solic S and Ivanković M 2023 Effects of different surface treatments of woven glass fibers on mechanical properties of an acrylic denture base material *Int. J. Mol. Sci.* **24** 909
[34] Petersen H N, Almdal K, Brøndsted P, Kusano Y and Sørensen B F 2017 Investigation of sizing - from glass fibre surface to composite interface *DTU Nanotech 34th Ris) International Symposium on Materials Science* 34, 333–40
[35] Deng J, Song Y, Lan Z, Xu Z, Chen Y, Yang B and Hao H 2022 The surface modification effect on the interfacial properties of glass fiber-reinforced epoxy: a molecular dynamics study *Nanotechnology Reviews* **11** 1143–57

[36] Nituica M, Oprea O, Stelescu M D, Sonmez M, Georgescu M, Alexandrescu L and Motelica L 2023 Polymeric biocomposite based on thermoplastic polyurethane (TPU) and protein and elastomeric waste mixture *Materials* **16** 5279
[37] Benlikaya R, Slobodian P and Riha P 2013 Enhanced strain- dependent electrical resistance of polyurethane composites with embedded oxidized multiwalled carbon nanotube networks *J. Nanomater.* **2013** 327597
[38] Benlikaya R, Slobodian P, Riha P, Puliyalil H, Cvelbar U and Olejnik R 2022 Ammonia plasma-treated carbon nanotube/epoxy composites and their use in sensing applications *Express Polymer Letters* **16** 85–101
[39] Shepherd J J 2022 *Analytical Techniques to Observe The Chemical Biodegradation of Thermoplastic Polyurethane Resins: FTIR, NMR, and SEM.* University of California San Diego Retrieved from https://escholarship.org/uc/item/4537j5hq
[40] Ahad N A 2020 A Recent blend of thermoplastic polyurethane *IOP Conf. Series: Materials Science and Engineering* 957
[41] Abiko K, Kato Y, Hohjo H, Kishida Y and Sudo E 2019 Raman imaging of residual stress distribution in epoxy resin and metal interface *J. Raman Spectrosc.* **51** 193–200
[42] Zhou J, Zou J, Han L, Long H, Zhao Y and Qi W 2024 Study on the properties and mechanism of orientated PAN/TPU composite materials using Raman spectroscopy *J. Appl. Polym. Sci.* **141** e56239
[43] Bruckmoser K and Resch K 2014 Investigation of ageing mechanisms in thermoplastic polyurethanes by means of ir and raman spectroscopy *Macromolecular Symposia* **339** 70–83
[44] Weakley A T, Warwick P C T, Bitterwolf T E and Aston D E 2012 Multivariate analysis of micro-raman spectra of thermoplastic polyurethane blends using principal component analysis and principal component regression *Appl. Spectrosc.* **66** 1269–78
[45] Shen R, Quan Y and Wan Q 2022 Thermal stability and flame retardancy of epoxy/synthetic fiber composites ed S Mavinkere Rangappa, J Parameswaranpillai, S Siengchin and S Thomas *Handbook of Epoxy/Fiber Composites* (Springer)
[46] Qiao Y, Das O, Zhao S N, Sun T S, Xu Q and Jiang L 2020 Pyrolysis kinetic study and reaction mechanism of epoxy glass fiber reinforced plastic by thermogravimetric analyzer (TG) and TG–FTIR (Fourier-Transform Infrared) *Techniques Polymers* **12** 2739
[47] Petrović Z S, Zavargo Z, Flyn J H and Macknight W J 1994 Thermal degradation of segmented polyurethanes *J. Appl. Polym. Sci.* **51** 1087–95
[48] Cervantes-Uc J M, Moo Espinosa J I, Cauich-Rodríguez J V, Ávila-Ortega A, Vázquez-Torres H, Marcos-Fernández A and San Román J 2009 TGA/FTIR studies of segmented aliphatic polyurethanes and their nanocomposites prepared with commercial montmorillonites *Polym. Degrad. Stab.* **94** 1666–77